Original Article

Macrophage Scavenger Receptor-A–Deficient Mice Are Resistant Against Diabetic Nephropathy Through Amelioration of Microinflammation

Hitomi Kataoka Usui,[1] Kenichi Shikata,[1] Motofumi Sasaki,[1] Shinichi Okada,[1] Mitsuhiro Matsuda,[1] Yasushi Shikata,[1] Daisuke Ogawa,[1] Yuichi Kido,[1] Ryo Nagase,[1] Kosuke Yozai,[1] Sakiko Ohga,[1] Atsuhito Tone,[1] Jun Wada,[1] Motohiro Takeya,[2] Seikoh Horiuchi,[3] Tatsuhiko Kodama,[4] and Hirofumi Makino[1]

Microinflammation is a common major mechanism in the pathogenesis of diabetic vascular complications, including diabetic nephropathy. Macrophage scavenger receptor-A (SR-A) is a multifunctional receptor expressed on macrophages. This study aimed to determine the role of SR-A in diabetic nephropathy using SR-A–deficient (SR-A$^{-/-}$) mice. Diabetes was induced in SR-A$^{-/-}$ and wild-type (SR-A$^{+/+}$) mice by streptozotocin injection. Diabetic SR-A$^{+/+}$ mice presented characteristic features of diabetic nephropathy: albuminuria, glomerular hypertrophy, mesangial matrix expansion, and overexpression of transforming growth factor-β at 6 months after induction of diabetes. These changes were markedly diminished in diabetic SR-A$^{-/-}$ mice, without differences in blood glucose and blood pressure levels. Interestingly, macrophage infiltration in the kidneys was dramatically decreased in diabetic SR-A$^{-/-}$ mice compared with diabetic SR-A$^{+/+}$ mice. DNA microarray revealed that proinflammatory genes were overexpressed in renal cortex of diabetic SR-A$^{+/+}$ mice and suppressed in diabetic SR-A$^{-/-}$ mice. Moreover, anti–SR-A antibody blocked the attachment of monocytes to type IV collagen substratum but not to endothelial cells. Our results suggest that SR-A promotes macrophage migration into diabetic kidneys by accelerating the attachment to renal extracellular matrices. SR-A may be a key molecule for the inflammatory process in pathogenesis of diabetic nephropathy and a novel therapeutic target for diabetic vascular complications. *Diabetes* 56:363–372, 2007

From the [1]Department of Medicine and Clinical Science, Okayama University Graduate School of Medicine, Dentistry and Pharmaceutical Sciences, Okayama, Japan; the [2]Department of Cell Pathology, Postgraduate School of Medicine, Kumamoto University, Kumamoto, Japan; the [3]Department of Medical Biochemistry, Faculty of Medical and Pharmaceutical Sciences, Kumamoto University, Kumamoto, Japan; and the [4]Laboratory for System Biology and Medicine, The Research Center for Advanced Science and Technology, the University of Tokyo, Tokyo, Japan.

Address correspondence and reprint requests to Kenichi Shikata, MD, PhD, Department of Medicine and Clinical Science, Okayama University Graduate School of Medicine, Dentistry and Pharmaceutical Sciences, 2-5-1 Shikata-cho, Okayama 700-8558, Japan. E-mail: shikata@md.okayama-u.ac.jp.

Received for publication 19 March 2006 and accepted in revised form 13 November 2006.

AGE, advanced glycation end product; FBS, fetal bovine serum; HUVEC, human umbilical vein endothelial cell; ICAM-1, intercellular adhesion molecule-1; IL, interleukin; mAb, monoclonal antibody; MMI, mesangial matrix index; NIH, National Institutes of Health; OPN, osteopontin; PAM, periodic acid-methenamine silver; PMA, phorbol myristate acetate; RAGE, receptor for AGE; SR-A, scavenger receptor-A; TBS, Tris-buffered saline; TGF, transforming growth factor; UACR, urinary albumin–to–creatinine ratio.

DOI: 10.2337/db06-0359

Diabetic nephropathy is a major cause of end-stage renal failure worldwide. The postulated pathogenesis in the progression of diabetic nephropathy includes activation of protein kinase C (1), acceleration of the polyol pathway, overexpression of transforming growth factor (TGF)-β (2), and accumulation of advanced glycation end products (AGEs) (3,4). Recently, accumulated data have emphasized the critical roles of inflammatory process in development of diabetic nephropathy (5,6), suggesting that microinflammation is a common mechanism in pathogenesis of diabetic vascular complications. Furuta et al. (7) reported that infiltration of mononuclear cells is prominent in the glomeruli of patients with diabetic nephropathy. Our group also reported the accumulation of macrophages and increased expression of cell adhesion molecules in renal biopsy specimens from patients with diabetic nephropathy (8). We pointed out that intercellular adhesion molecule-1 (ICAM-1) is overexpressed on endothelial cells and mediates macrophage infiltration in diabetic kidney (8,9). Furthermore, we demonstrated that blockade of the inflammatory axis of ICAM-1 activation to macrophage infiltration ameliorates diabetic nephropathy using ICAM-1–deficient mice (10).

Macrophage scavenger receptor-A (SR-A), cloned by Kodama in 1990, is a multi-ligand and multifunctional receptor expressed mainly on macrophages (11,12). A number of studies have established the important roles of SR-A in the atherosclerotic process. SR-A is involved in foam cell formation, activation of macrophages, and adhesion of macrophages to atherosclerotic lesions (13–17). Recently, several investigators found that SR-A binds to AGEs (18). Uesugi et al. (19) revealed the presence of macrophages positive for AGE in glomerular lesions of patients with diabetic nephropathy. Furthermore, high glucose condition enhanced expression of SR-A on cultured human monocytes (20). However, the role of SR-A in diabetic microangiopathy remains unknown. The aim of this study is to determine the role of SR-A in diabetic nephropathy using SR-A–deficient (SR-A$^{-/-}$) mice. We induced diabetes in SR-A$^{-/-}$ mice by streptozotocin and compared the progression of renal injuries with SR-A$^{+/+}$ mice. In addition, we conducted microarray and cell adhesion assays to determine the role of SR-A in the adhesion and infiltration of macrophages.

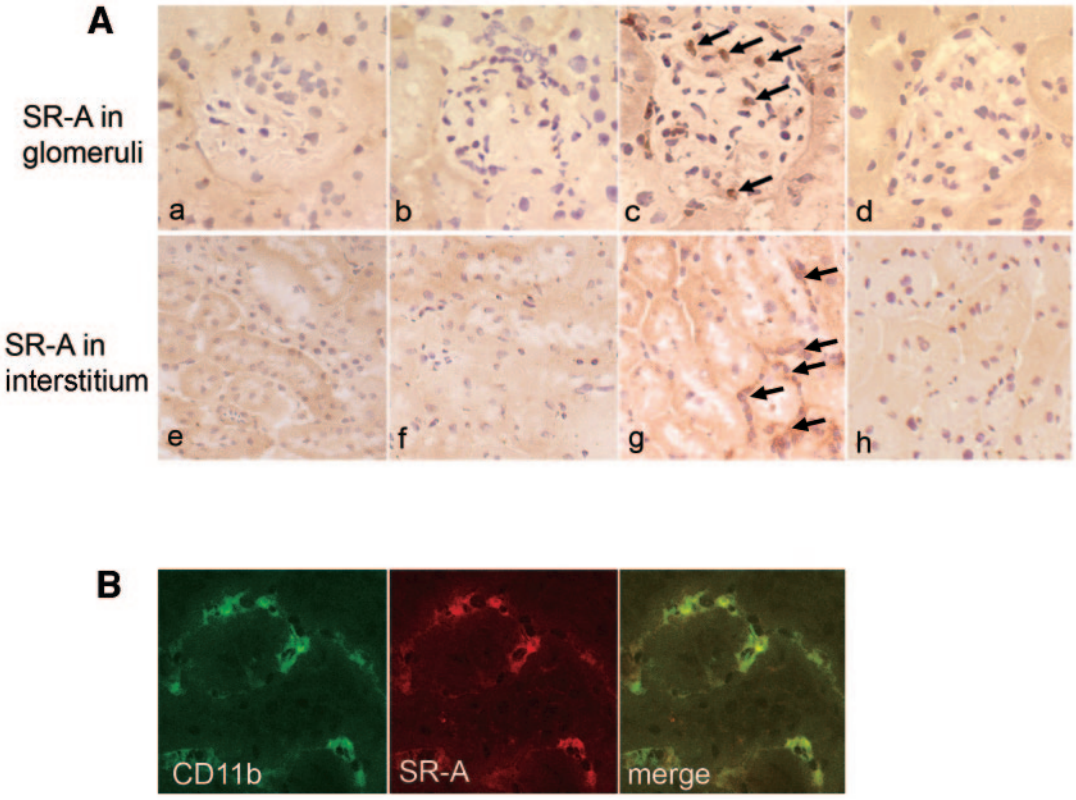

FIG. 1. *A*: SR-A expression in glomeruli (*a–d*) and interstitium (*e–h*). SR-A was expressed only in diabetic SR-A$^{+/+}$ mice (*c* and *g*). Nondiabetic SR-A$^{+/+}$ mice (*a* and *e*), nondiabetic SR-A$^{-/-}$ mice (*b* and *f*), and diabetic SR-A$^{-/-}$ mice (*d* and *h*) did not express SR-A. Original magnification: *a–d* (×400), *e–h* (×200). *B*: Double staining of SR-A and CD 11b. SR-A (red) and CD11b (green) were detected in diabetic SR-A$^{+/+}$ mice kidney. They were mostly co-expressed in merged picture.

RESEARCH DESIGN AND METHODS

Male mice deficient in macrophage type-I and type-II class A scavenger receptors (SR-A$^{-/-}$ mice, C57BL/6J background) were obtained from Fuji Gotenba Research Laboratories (Chugai Pharmaceutical, Shizuoka, Japan). These mice were generated by disrupting exon 4 of the SR-A gene, which is essential for the formation of functional trimetric receptors (15). Wild-type C57BL/6J mice (SR-A$^{+/+}$ mice) were used as control. SR-A$^{-/-}$ mice showed normal growth with normal white blood cell count and differential count.

Experimental protocol

Eight-week-old male C57BL/6J mice (SR-A$^{-/-}$ and SR-A$^{+/+}$mice) were divided into four groups (n = 15 each): *1*) diabetic SR-A$^{-/-}$ mice (DM-KO), *2*) diabetic SR-A$^{+/+}$ mice (DM-WT), *3*) nondiabetic SR-A$^{-/-}$ mice (ND-KO), and *4*) nondiabetic SR-A$^{+/+}$ mice (ND-WT). Diabetes was induced by peritoneal injection of streptozotocin (Sigma Chemical, St. Louis, MO) at 200 mg/kg in citrate buffer (pH 4.5). Mice of the nondiabetic group were injected with citrate buffer. All mice had free access to standard diet and tap water. All procedures were performed according to the Guidelines for Animal Experiments at Okayama University Medical School, Japanese Government Animal Protection and Management Law (No. 105) and Japanese Government Notification on Feeding and Safekeeping of Animals (No. 6). Mice were killed at 6 months after induction of diabetes. The harvested kidneys were weighed and fixed in 10% formalin for periodic acid-methenamine silver (PAM) and Masson trichrome staining, and parts of the remaining tissues were embedded in optimal cutting temperature compound (Sakura Finetechnical, Tokyo) and frozen immediately in acetone cooled on dry ice. Other remaining tissues were snap frozen in liquid nitrogen and stored at −80°C.

Metabolic tests

Systolic blood pressure, A1C, total cholesterol, and serum creatinine were measured once every month. Blood pressure was measured by the tail-cuff method (Softron, Tokyo). Blood glucose was measured periodically by the glucose oxidase method. A1C was measured by latex-agglutination assay. Total cholesterol was measured by cholesterol oxidase-HDAOS [*N*-(2-hydroxy-3-sulfopropyl)-3,5-dimethoxyaniline, sodium salt] method. Serum lipid peroxides were measured by thiobarbituric acid method at 6 months. Creatinine was measured by enzymatic method, and creatinine clearance (CCr) was calculated. Urine was collected over 24 h with each mouse individually housed in a metabolic cage and provided with food and water ad libitum. Urinary albumin concentration was measured using nepherometry. Results were normalized to the urinary creatinine levels and expressed as urinary albumin–to–creatinine ratio (UACR).

Light microscopy

PAM- and Masson trichrome–stained sections were analyzed. To evaluate glomerular size, we examined 10 randomly selected glomeruli in the cortex per animal under high magnification (×400) at 1, 3, and 6 months after induction of diabetes. The area of the glomerular tuft and mesangial matrix index (MMI) were measured using PhotoShop software version 6 (Adobe Systems, San Jose, CA) and National Institutes of Health (NIH) image software version 1.62, as described previously (10). MMI was defined as the PAM-positive area in the tuft area, calculated using the following formula: MMI = (PAM positive area)/(tuft area), at 6 months. The results were expressed as means ± SE (square micrometer for tuft area; arbitrary unit for MMI).

Immunohistochemical staining

Immunoperoxidase and immunofluorescent staining were performed using the methods described previously (10).

Immunoperoxidase staining. Fresh frozen sections were cut at 4-μm thickness by a cryostat. To examine the expression of SR-A in kidney tissues, rat anti-mouse SR-A I and II (2F8) monoclonal antibody (mAb) (Serotec, Raleigh, NC) was applied, followed by biotin-labeled goat anti-rat IgG antibody (Jackson Immunoresearch Laboratories, West Grove, PA). Avidin-biotin coupling reaction was performed on sections using Vectastain Elite kit (Vector Laboratories, Burlingame, CA). To evaluate infiltration of macrophages, we applied rat anti-mouse monocyte/macrophage (F4/80) mAb (Serotec), followed by biotin-labeled goat anti-rat IgG antibody. We examined 10 glomeruli per animal and counted F4/80-positive cells. The average number of positive cells per glomerulus and interstitial tissue (number per square millimeter) were used for the estimation. To evaluate TGF-β expression, TGF-β1/2/3 rabbit polyclonal antibody (Santa Cruz Biotechnology, Santa Cruz, CA) was applied, followed by biotin-labeled donkey anti-rabbit IgG antibody (Jackson Immunoresearch Laboratories). Glomerular TGF-β–positive area was estimated in 10 glomeruli per animal, using NIH Image. Biotin-conjugated anti-AGE mAb (clone 6D12) (Trans Genic, Kumamoto, Japan) was used to recognize carboxymethyllysine.

Immunofluorescent staining. For double staining, 2F8 mAb followed by

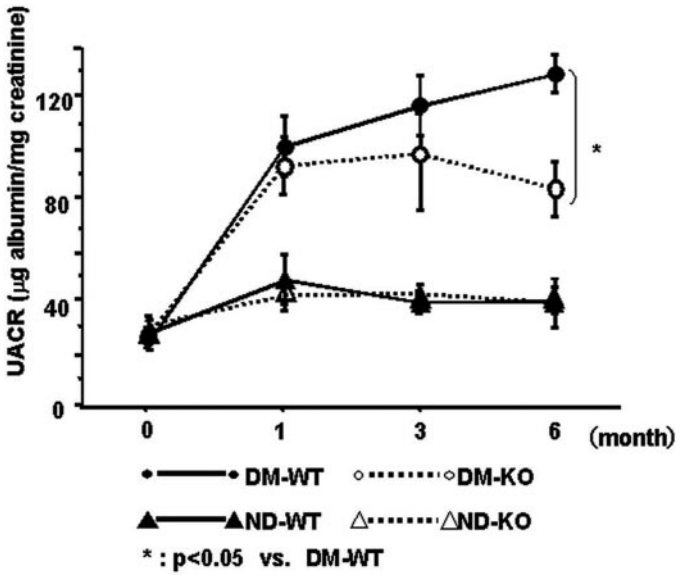

FIG. 2. Time course of UACR. UACR of diabetic SR-A$^{+/+}$ mice (DM-WT, closed circle) increased progressively, whereas it was suppressed in diabetic SR-A$^{-/-}$ mice (DM-KO, open circle). UACR of nondiabetic SR-A$^{+/+}$ mice (ND-WT, closed triangle) and nondiabetic SR-A$^{-/-}$ (ND-KO, open triangle) did not increase remarkably. Data are means ± SE. *$P < 0.05$ for DM-WT versus DM-KO.

Texas red–conjugated anti-rat IgG antibody (Cappel, Aurola, OH) and Alexa Fluor 488 anti-mouse CD11b (BioLegend, San Diego, CA) were applied. To clarify the difference in mesangial matrix proteins, we used rabbit anti–type IV collagen antibody (Chemicon, Temecula, CA), followed by fluorescein isothiocyanate–labeled anti-rabbit IgG (Jackson Immunoresearch Laboratories). Goat anti-receptor for AGE (RAGE) antibody (Chemicon) was applied, followed by fluorescein isothiocyanate–labeled donkey anti-goat IgG antibody (Jackson Immunoresearch Laboratories). Fluorescence pictures were obtained using confocal laser fluorescence microscope (LSM-510; Carl Zeiss, Jena) in the Central Research Laboratory, Okayama University Medical School. Quantification of type IV collagen and RAGE immunofluorescence intensity was performed as described previously (10). Briefly, image files were opened using NIH Image, and intensity of expression was calculated using the formula, x (density) × positive area (μm^2). The expression of type IV collagen in each glomerulus was estimated as the ratio to the mean expression in ND-WT. Ten glomeruli per animal were evaluated.

Affymetrix oligonucleotide microarray analysis

Total RNA was extracted from each specimen of renal cortex using RNeasy kit (Qiagen, Valencia, CA) at 3 months. Preparation of cRNA and hybridization of probe arrays (Mouse Genome 430 2.0) were performed according to the manufacturer's instructions (Affymetrix, Santa Clara, CA). These arrays contain probe sets for >45,000 transcripts. After hybridization, microarrays were washed, scanned, and analyzed with the GENECHIP software Microarray Suite version 5.0 (Affymetrix). The criteria for selecting genes that were induced or reduced by diabetic state were as follows: *1*) genes whose flags were "present"; *2*) ratio of expression level of DM-WT >2 or <0.5 of that of ND-WT; and *3*) $P < 0.05$. We then selected 107 genes for further analysis. All raw data values were replaced to log base 2 and subjected to hierarchical clustering. Analysis was performed using Cluster and Tree View hierarchical clustering software developed by Eisen et al. (21) (http://rana.lbl.gov/).

Similarity was measured by standard correlation of the average difference for each gene, which was normalized to itself by making a synthetic positive control for that gene and dividing all measurements for that gene by this positive control, assuming it was at least 1.0. This synthetic control was the median of the gene's expression values over all the samples. Each row represents a single gene, and each column represents an experimental sample. The ratio of the abundance of transcripts of each gene to the median abundance of the gene's transcript is represented by a color in the corresponding sample in the matrix. Green squares indicate transcript levels below the median; red squares indicate transcripts levels above the median.

Functional profiling of differentially regulated genes in DM-WT and DM-KO was performed based on the Gene Ontology Consortium (http://www.geneontology.org) terms (22). The gene annotation procedure was performed using The Database for Annotation, Visualization, and Integrated Discovery 2.1 by the National Institute of Allergy and Infectious Disease (http://david.abcc.ncifcrf.gov/) (23). Out of the three available Gene Ontology Consortium ontologies, the biological process annotation is presented in this article.

Quantitative analysis of osteopontin by real-time RT-PCR

Total RNA was extracted from each specimen of renal cortex using RNeasy kit (Qiagen) at 3 months. Single-strand cDNA was synthesized from the extracted RNA using an RT-PCR kit (Perkin Elmer, Foster City, CA) according to the manufacturer. To evaluate mRNA expression of osteopontin (OPN) in renal cortex, quantitative real-time RT-PCR was performed using Light Cycler and Light Cycler-FastStart SYBR Green1 (Roche Diagnostics, Tokyo). After the addition of primers (final concentration 0.3 μmol/l), $MgCl_2$ (3 mmol/l), and template DNA to the maser mix, 45 cycles of denaturation (95 °C for 10 s), annealing (62 °C for 10 s), and extension (72°C for 6 s) were performed. To determine the specificity of each primer set, melting curve analysis was performed. Accumulated levels of fluorescence were analyzed by the fit-point method after melting curve analysis. The mRNA expression level of OPN was normalized by β-actin in each sample, calculating the relative expression ratio. For amplification of the cDNA, the following oligonucleotide primers specific for mouse OPN (GenBank accession no. NM_009263) and mouse β-actin (GenBank accession no. NM_007393) were used: OPN, sense 5′-TC CAATCGTCCCTACAGTCG-3′ and antisense 5′-CAACAGGGATGACATCGAG G-3′; and β-actin, sense 5′-CCTGTATGCCTCTGGTCGTA-3′ and antisense 5′-CCATCTCCTGCTCGAAGTCT-3′ (Nihon Gene Research Labs, Sendai, Japan). Each experiment was performed twice.

Adhesion assay

Cell culture. Human umbilical vein endothelial cells (HUVECs) were purchased from Asahi Techno Glass (Tokyo) and seeded on a gelatin-coated cell culture flask (Becton Dickinson, Franklin Lakes, NJ) with the EGM-Endothelial Cell Medium Bullet kit (Clontech Laboratories, Palo Alto, CA). HUVECs were cultured at 37°C in humidified air containing 5% CO_2. The human monocytic cell line THP-1 (Japanese Collection of Research Bioresources, Tokyo) was cultured in RPMI-1640 (Dainippon Pharmaceutical, Osaka, Japan) supplemented with 10% fetal bovine serum (FBS) (Clontech).

Cell-to-substrate adhesion assay. THP-1 to be assayed for adhesion was activated by phorbol myristate acetate (PMA; 50 ng/ml) for 2 h and suspended in RPMI with 4% FBS. Mouse anti-human SR-A mAb (C6) (a gift from Kumamoto University, Kumamoto, Japan) (20,24) and anti-human integrin β_1 adhesion-nonblocking mAb (Chemicon) were used for the assay. It was designed to observe their inhibitory effect on THP-1 adhesion onto type IV collagen and performed as follows. It was raised in SR-A–knockout mice by immunizing human SR-A and shown to act as an anti–SR-A–neutralizing antibody (20,24), and anti-human integrin β_1 adhesion-nonblocking mAb (Chemicon) was performed as follows. Cells were preincubated with PBS (control) and specific mAb (10 μg/ml) for 30 min at 4°C with mAb alone or in combination with chelators (5 mmol/l EDTA). Then 5.0×10^5 cells/each well were cultured on the Biocoat collagen IV cellware 24-well plate (Becton Dickinson) at 37°C and 5% CO_2. Adhesion was determined after 1 h of

TABLE 1
Metabolic data of four groups at 6 months

	ND-WT	ND-KO	DM-WT	DM-KO
Blood pressure (mmHg)	96.8 ± 3.9	99.7 ± 7.6	106.0 ± 2.7	110.1 ± 1.5
Body weight (g)	31.0 ± 0.7	32.2 ± 0.9	21.5 ± 0.9*†	25.2 ± 1.2‡§
Kidney weight (mg/g body wt)	10.3 ± 0.7	12.4 ± 0.4	21.9 ± 1.0*†	19.1 ± 1.6‡§
A1C (%)	3.7 ± 0.1	3.7 ± 0.2	9.9 ± 0.5*†	9.6 ± 0.2*†
CCr (ml · min^{-1} · g body wt^{-1})	6.5 ± 1.3	5.5 ± 0.8	25.2 ± 3.9*†	21.0 ± 3.8*†
Lipid peroxides (nmol/ml)	2.8 ± 0.3	4.5 ± 0.9	22.6 ± 6.5†‡	9.6 ± 1.8‡¶
Total cholesterol (mg/dl)	84.0 ± 1.4	80.0 ± 3.8	125.2 ± 8.3‡§	94.0 ± 3.9‡¶

Data are means ± SE. *$P < 0.0001$ vs. ND-WT. †$P < 0.0001$ vs. ND-KO. ‡$P < 0.05$ vs. ND-WT. §$P < 0.05$ vs. ND-KO. ¶$P < 0.05$ vs. DM-WT.

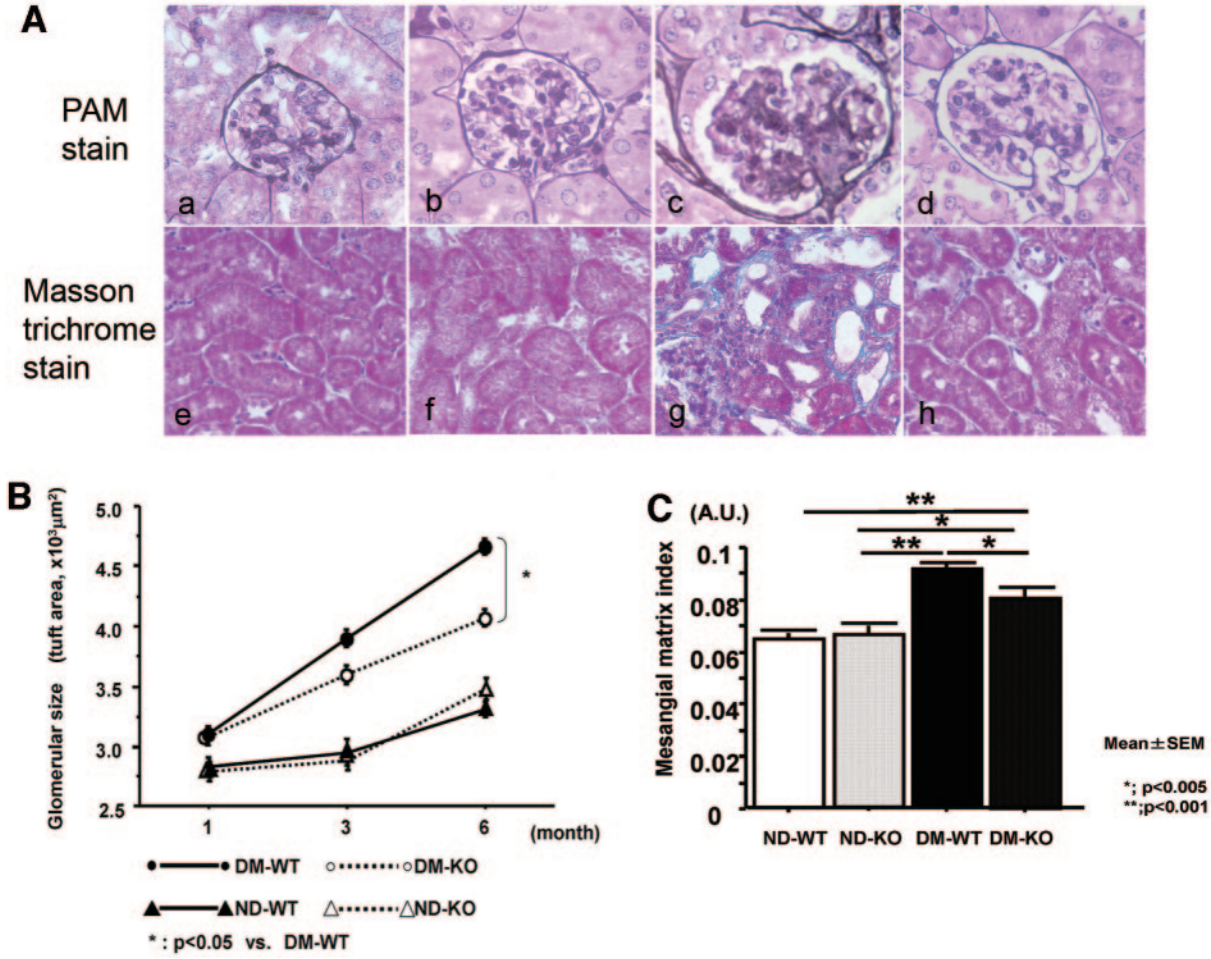

FIG. 3. *A*: PAM (*a*–*d*) and Masson trichrome (*e*–*h*) staining of the kidney. Glomerular hypertrophy and mesangial matrix expansion (*c*) and interstitial fibrosis (*g*) of diabetic SR-A$^{+/+}$ mice (DM-WT) were ameliorated in diabetic SR-A$^{-/-}$ mice (DM-KO; *d* and *h*). *a* and *e*: Nondiabetic SR-A$^{+/+}$ mice (ND-WT). *b* and *f*: Nondiabetic SR-A$^{-/-}$ mice (ND-KO). Original magnification ×400 (*a*–*d*) and ×200 (*e*–*h*). *B*: Time course of glomerular size. Glomerular size increased progressively in DM-WT (closed circle) and gradually in DM-KO (open circle). ND-WT (closed triangle) and ND-KO (open triangle) did not show remarkable change. Data are means ± SE. *$P < 0.05$ for DM-WT versus DM-KO. $n = 4$ in each group. *C*: MMI at 6 months. MMI, calculated by PAM-positive area in the tuft area, was increased in DM-WT and suppressed in DM-KO. Data are means ± SE. *$P < 0.005$; **$P < 0.001$.

incubation (±mAb, ±chelator). Unbound cells were removed by washing three times with PBS, and adherent cells were fixed by 3.7% formalin. Adherent cells were pictured using an inverted microscope (IX71) (Olympus, Tokyo). The number of adherent cells (cells/135 μm^2) was expressed relative to the mean number of the control.

Cell-to-cell adhesion assay. Cell-to-cell adhesion assay was performed based on the method reported by Kataoka et al. (25). Briefly, HUVECs were seeded onto a gelatin-coated 24-well cell culture cluster (Costar, Corning, NY) until confluence. HUVECs were then stimulated with human interleukin (IL)-1β (5 ng/ml; Genzyme, Cambridge, MA) for 6 h and subsequently overlayered with 20 μl of culture medium containing PMA-activated THP-1 (5.0×10^5 cells/ml). THP-1 was preincubated with mAb (5 μg/ml) and control (PBS) for 30 min. Antibodies were mouse anti-human integrin-β_2 adhesion-blocking mAb (Chemicon), anti-human integrin-β_1 adhesion-nonblocking mAb (Chemicon), and mouse anti-human SR-A mAb (C6). Adhesion was determined after a 1-h incubation period, as stated above. Adherent cells were observed and pictured using an inverted microscope (IX71). The number of adherent cells was expressed relative to the mean number of the control.

Immunofluorescence microscopy assay of cells

Immunofluorescence microscopy assay was performed as described previously (26). The above-mentioned cell-cell adhesion assay was performed on gelatin-coated coverslips (Matsunami Glass, Tokyo). HUVECs and adherent THP-1 were fixed in 3.7% paraformaldehyde in PBS for 15 min, washed with PBS, permeabilized with 0.25% Triton X-100 containing Tris-buffered saline (TBS-T) for 15 min, and blocked with 2% BSA in TBS-T. Incubation with mouse anti-human CD68 mAb (Dako, Glostrup, Denmark) was performed for 1 h. After three washes, the cells were incubated with Alexa Fluor 488 goat anti-mouse IgG antibody (Invitrogen, Carlsbad, CA). Actin filaments were visualized by Texas red–conjugated phalloidin (Invitrogen). Fluorescence pictures were obtained using an inverted microscope (IX71).

Statistical analysis

All data are expressed as means ± SE. One-way ANOVA followed by the Scheffe method was used to compare the mean of group data. A P value <0.05 denoted the presence of a statistically significant difference.

RESULTS

Expression of SR-A in the kidney. We observed SR-A expression in the kidneys of four animal groups. SR-A was not expressed in renal tissues of ND-WT and SR-A$^{-/-}$ mice but was detected in glomeruli and interstitium of DM-WT, in accord with macrophages (Fig. 1*A*). SR-A (red) and CD11b (green) were detected in DM-WT kidney. They were mostly co-expressed in merged picture (Fig. 1*B*). No signal of SR-A was detected in DM-KO (data not shown).

Metabolic data and time course of *UACR*. UACR increased progressively during the 6-month observation period in DM-WT. DM-KO showed lower UACR at 3 months. UACR at 6 months (DM-WT vs. DM-KO, 129.5 ± 7.37 vs. 83.5 ± 9.64 μg/mg) was significantly reduced in DM-KO (Fig. 2). The other metabolic data are summarized in Table 1. At 6 months, there was no significant difference in systolic blood pressure between the groups. Although

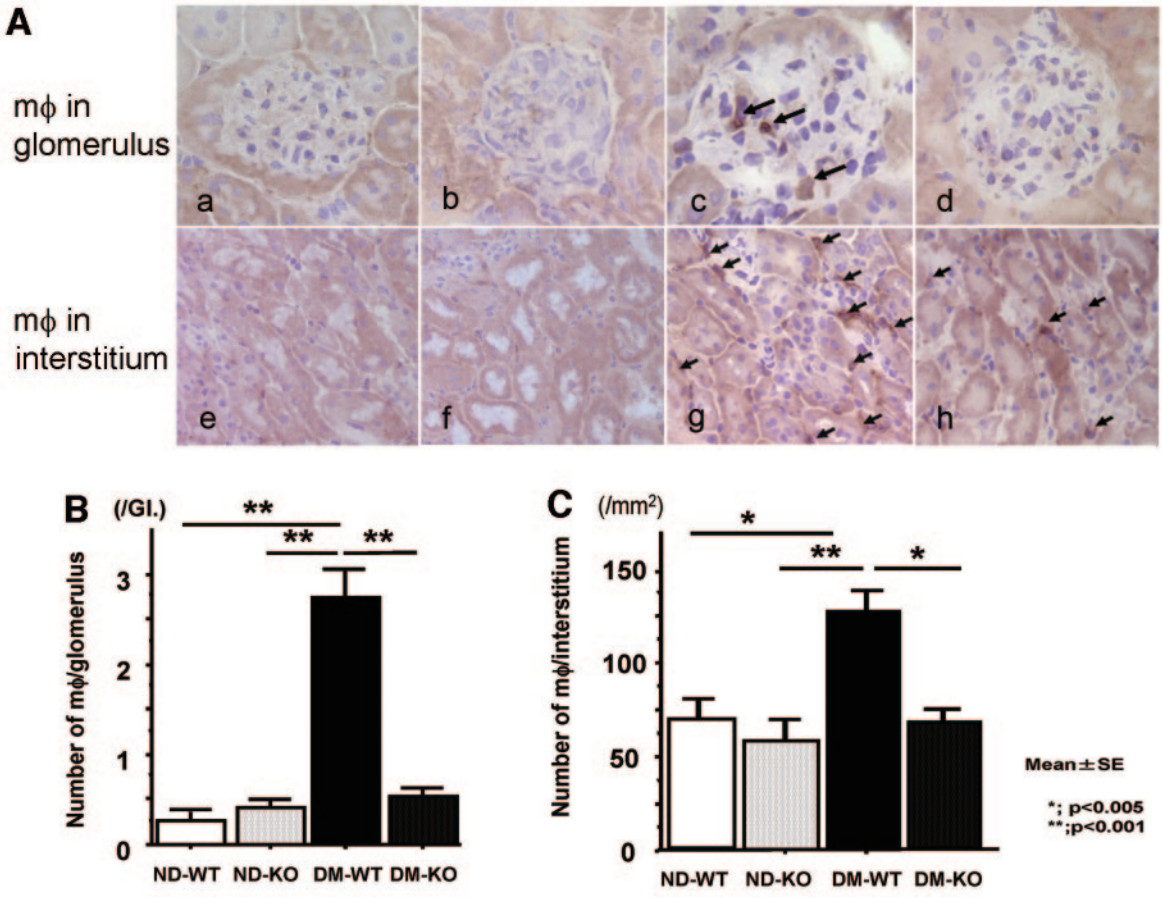

FIG. 4. ***A*: Macrophage infiltration into the kidney. *a–h*: Macrophage (arrows) infiltration into glomeruli (*c*) and interstitium (*g*) was remarkable in diabetic SR-A$^{+/+}$ mice (DM-WT), whereas it was minimal in diabetic SR-A$^{-/-}$ mice (DM-KO; *d* and *h*). *a* and *e*: Nondiabetic SR-A$^{+/+}$ mice (ND-WT). *b* and *f*: Nondiabetic SR-A$^{-/-}$ mice (ND-KO). Original magnification ×400 (*a–d*) and ×200 (*e–h*). *B*: The number of intraglomerular macrophages. Data are means ± SE. ***P* < 0.001. *C*: The number of macrophages in interstitium. Data are means ± SE. **P* < 0.005; ***P* < 0.001.**

body weight of diabetic mice was decreased compared with nondiabetic mice, body weight of DM-KO was higher than DM-WT. Kidney weight per body weight was lower in DM-KO compared with DM-WT. There were no differences in A1C and CCr between DM-KO and DM-WT. Lipid peroxide was increased in DM-WT and significantly reduced in DM-KO. Total cholesterol was increased in DM-WT and slightly reduced in DM-KO.

Light microscopy. Glomerular hypertrophy progressed constantly in DM-WT. At 3 months, DM-KO presented lower glomerular size compared with DM-WT. At 6 months, glomerular size of DM-KO was significantly lower than DM-WT (DM-WT vs. DM-KO, $4.6 \times 10^3 \pm 79.3$ vs. $3.9 \times 10^3 \pm 79.9$ μm^2; Fig. 3*A*, *a–d*, and *B*). Quantitative analysis showed that MMI, which indicated mesangial expansion, was significantly larger in DM-WT than in DM-KO (DM-WT vs. DM-KO, 0.092 ± 0.02 vs. 0.081 ± 0.003 arbitrary units [AU]; Fig. 3*C*). In addition, Masson trichrome-stained sections showed that interstitial fibrosis was significant in DM-WT but mild in DM-KO (Fig. 3*A*, *e–h*).

Macrophage infiltration in the kidney. The number of macrophages in the glomeruli was remarkably high in DM-WT compared with nondiabetic mice. Interestingly, macrophage infiltration into glomeruli was markedly suppressed in DM-KO to a level similar to that in nondiabetic mice (DM-WT vs. DM-KO, 2.7 ± 0.19 vs. 0.6 ± 0.08; Fig. 4*A*, *a–d*, and *B*). Similarly, macrophage infiltration into the interstitium was increased in DM-WT but suppressed in DM-KO to a level similar to that in nondiabetic mice (Fig. 4*A*, *e–h*, and *C*).

Expression of TGF-β and type IV collagens. Expansion of the TGF-β–positive area was evident in glomeruli of DM-WT compared with nondiabetic mice. In contrast, the TGF-β–positive area was significantly reduced in DM-KO (DM-WT, 315.6 ± 31.2 μm^2; DM-KO, 122.5 ± 26.9 μm^2; Fig. 5*A*, *a–d*, and *B*). Furthermore, the intensity of type IV collagen fluorescence in glomeruli was slightly higher in DM-WT than in DM-KO (DM-WT, 1.488; DM-KO, 1.362 AU, Fig. 5*A*, *e–h*, and *C*).

Expression of RAGE and AGE. RAGE expression and AGE deposition were increased in both DM-WT and DM-KO without significant difference between two groups. RAGE was expressed in glomeruli, and AGE deposition was increased in glomeruli and interstitium of the diabetic kidney (Fig. 5*D*).

Gene expression analysis by microarray. We examined gene expression profiles of four groups. We identified 107 genes; the ratio of expression level of DM-WT was >2 or <0.5 of that of ND-WT. Of 107 genes, hierarchical clustering identified 48 genes that were significantly upregulated only in DM-WT but not remarkable in DM-KO (cluster 4; Fig. 6*A*). Functional annotation of these 48 genes revealed that the most significant functions of them were related to the immune or inflammatory process: response to stimulus, defense response, and immune response (Fig. 6*B*). These genes contained several macrophage-specific genes, such as serum/glucocorticoid-regulated kinase and major

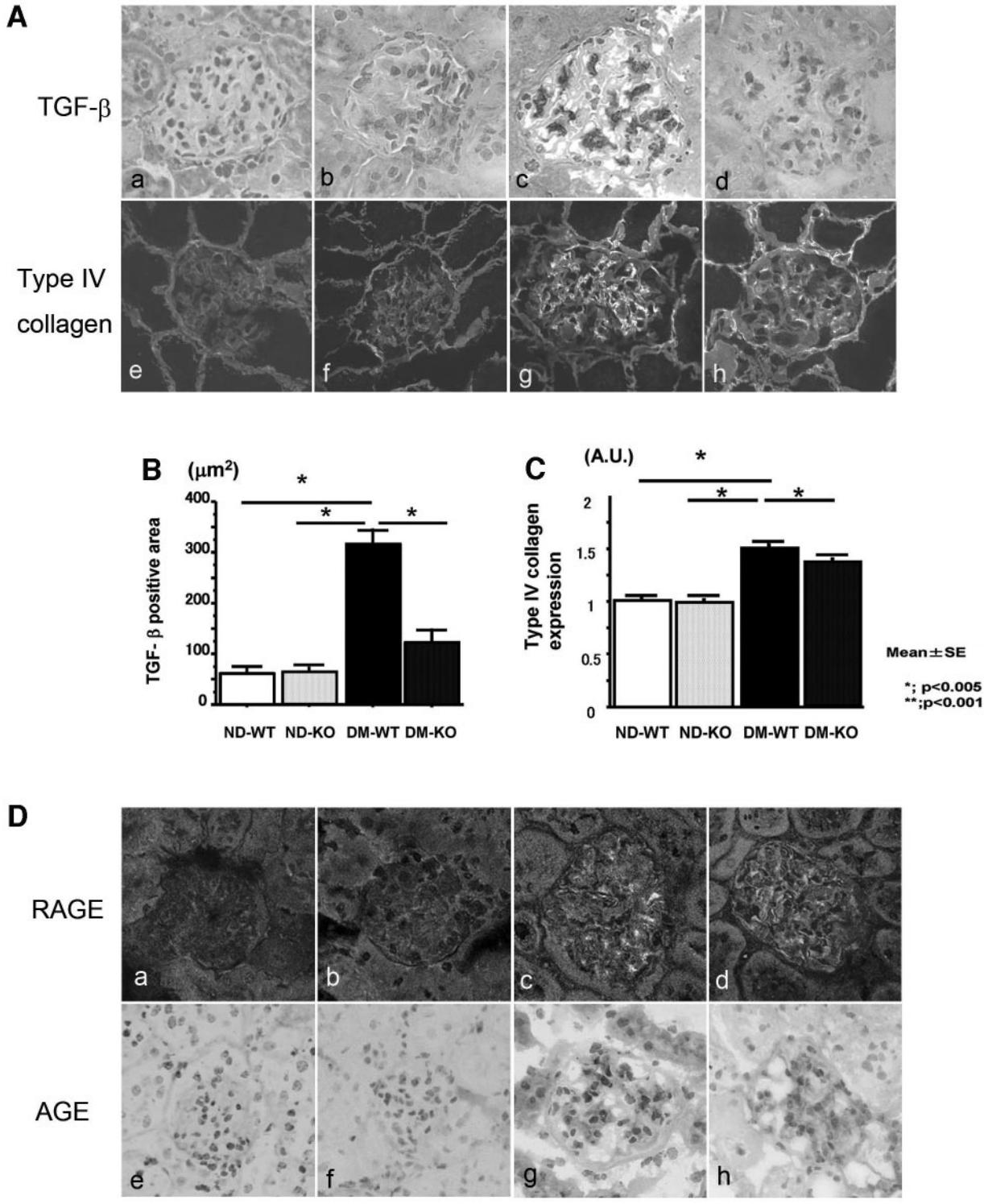

FIG. 5. ***A*****: Expression of TGF-β and type IV collagen in the kidney.** ***a–d*****: TGF-β was prominent in the glomeruli of diabetic SR-A$^{+/+}$ mice (DM-WT;** ***c*****) compared with diabetic SR-A$^{-/-}$ mice (DM-KO;** ***d*****).** ***e–h*****: Type IV collagen was slightly increased in DM-WT (*** ***g*****) compared with DM-KO (*** ***h*****).** ***a*** **and** ***e*****: nondiabetic SR-A$^{+/+}$ mice (ND-WT).** ***b*** **and** ***f*****: Nondiabetic SR-A$^{-/-}$ mice (ND-KO). Original magnification ×400.** ***B*****: TGF-β–positive area in glomeruli. Data are means ± SE. *$P < 0.005$.** ***C*****: Collagen IV–positive area in glomeruli (folds versus ND-WT). Data are means ± SE. *$P < 0.005$.** ***D*****: Expression of RAGE and AGE (carboxymethyllysine) in the kidney (RAGE,** ***a–d*****; AGE,** ***e–h*****). RAGE and AGE expression was increased in both diabetic mice without significant difference.** ***a*** **and** ***e*****, ND-WT;** ***b*** **and** ***f*****, ND-KO;** ***c*** **and** ***g*****, DM-WT; and** ***d*** **and** ***h*****, DM-KO. Original magnification ×400.**

histocompatibility complex class II, postulated previously (27).

OPN mRNA expression by real-time RT-PCR. Of 48 genes upregulated in DM-WT and not in DM-KO, we focused on OPN because it has been regarded as an important molecule in pathogenesis of diabetic nephropathy (28–31). In addition, it was one of the most abundantly expressed genes in renal cortex in our study. We performed real-time RT-PCR of the OPN gene. OPN mRNA expression was significantly higher in DM-WT (20 times

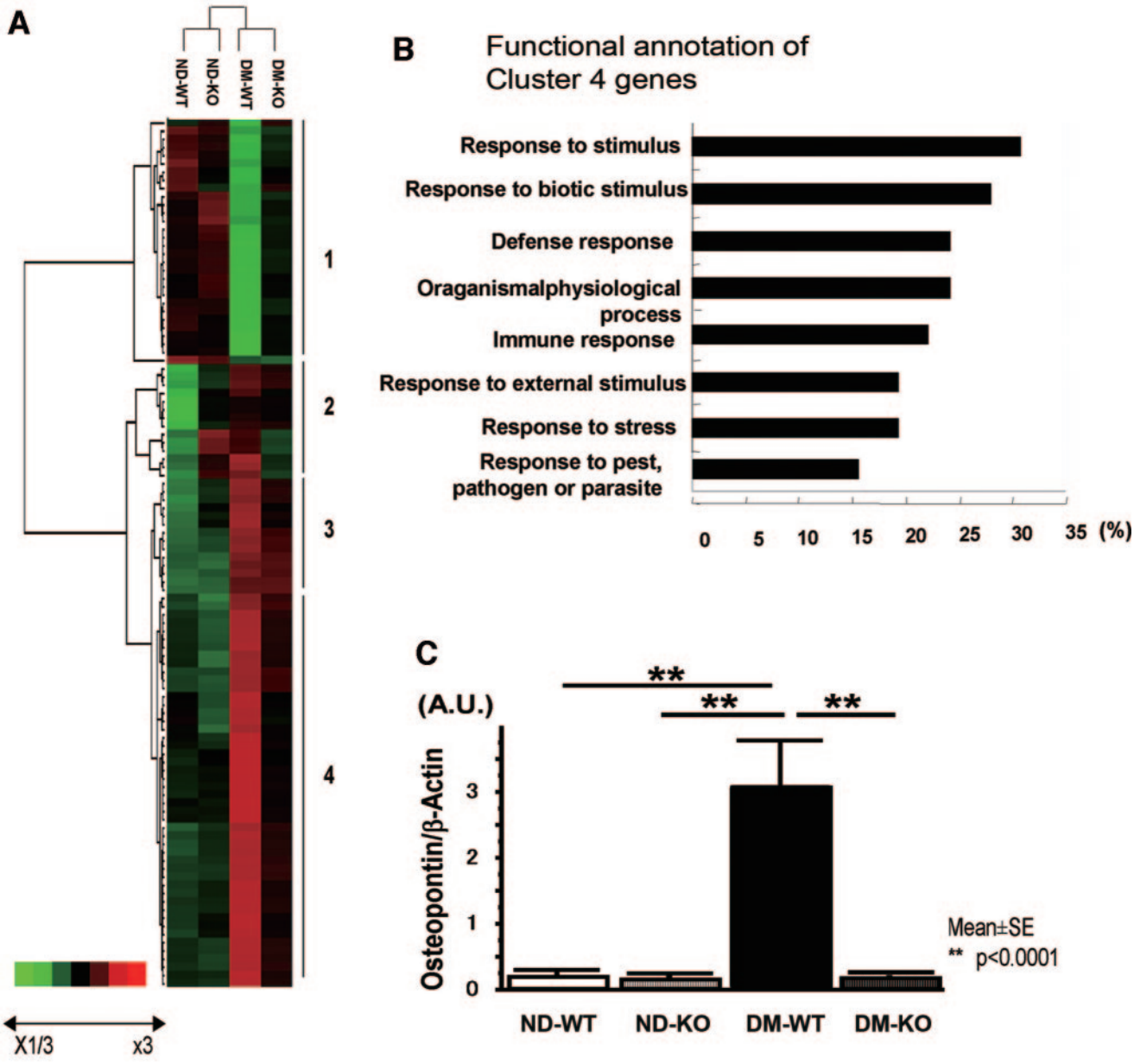

FIG. 6. Clustering of differently expressed genes in renal cortex and real-time RT-PCR of OPN. *A*: Cluster analysis of differentially expressed genes comparing nondiabetic SR-A$^{+/+}$mice (ND-WT), diabetic SR-A$^{+/+}$mice (DM-WT), diabetic SR-A$^{-/-}$ mice (DM-KO), and nondiabetic SR-A$^{-/-}$ mice (DM-KO). The dendrogram on the *left* of the cluster shows relatedness of gene expression change. On the *right* of the cluster diagram, four groups of genes (1–4) are identified based on their gene expression changes. *B*: Genes in cluster 4 (upregulated only in DM-WT, but not remarkable in DM-KO) were annotated with their biological function. *C*: The mRNA level of OPN was significantly increased in DM-WT and significantly reduced to nondiabetic level in DM-KO. Data are means ± SE. **$P < 0.0001$.

ND-WT) and reduced in DM-KO relative to the nondiabetic level (Fig. 6*C*).

Cell-substrate adhesion assay. The adhesion of macrophages to type IV collagen was detected without specific antibody (control). Adhesion diminished by 40% after the addition of anti-human SR-A mAb. Irrelevant antibody (anti-human integrin-β_2 adhesion-nonblocking mAb) reduced the adhesion only by 20% relative to the control. The addition of EDTA resulted in a significant blockade of adhesion without any antibody. Anti-human SR-A mAb further reduced adhesion by 50% relative to EDTA-added control. Irrelevant antibody reduced adhesion by 20% relative to the control (Fig. 7*A* and *B*).

Cell-cell adhesion assay. THP-1 adhesion to IL-1β–activated HUVEC monolayer was observed without blocking antibody (Fig. 7*C*). Mouse anti-human integrin-β_2 adhesion-blocking mAb blocked the adhesion by 50% of the control. In contrast, anti-human SR-A mAb and anti-human β1-integrin adhesion-nonblocking mAb reduced adhesion only by 20% of the control (Fig. 7*D*). Considered together, SR-A seems to contribute to macrophage transmigration into the subendothelial space (matrix).

DISCUSSION

Deficiency of SR-A resulted in amelioration of UACR, glomerular hypertrophy, macrophage infiltration, and overexpression of TGF-β in the kidneys in diabetic mice without change of blood glucose and blood pressure levels. Interestingly, these results were quite similar to

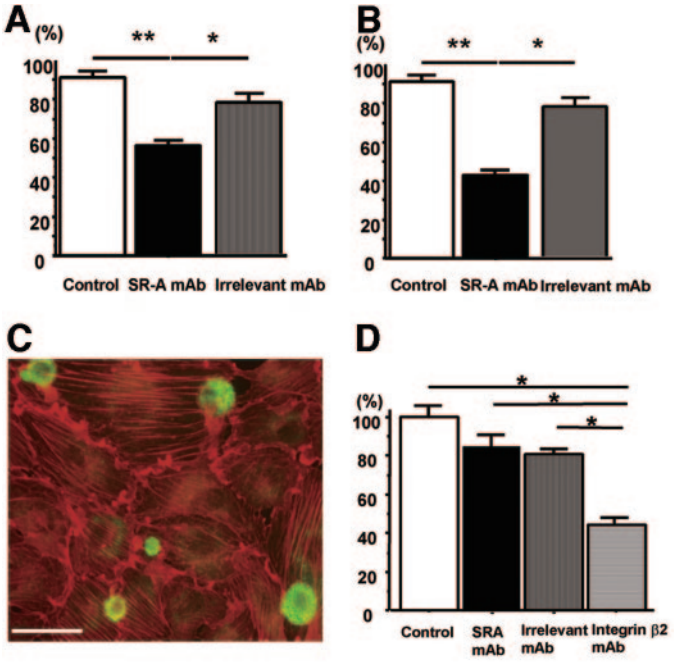

FIG. 7. Cell to substrate/cell adhesion assay. *A*: Without EDTA, the adhesion of macrophages to type IV collagen was reduced with anti-human SR-A mAb. *B*: With EDTA, anti-human SR-A mAb furthermore reduced adhesion compared with control. *C*: Immunohistochemistry of THP-1 (green) adhesion on IL-1β–activated HUVEC monolayer (red). Scale bar = 50 μm. Original magnification ×400. *D*: Anti-human SR-A mAb did not show marked inhibition of SR-A attachment. Data are means ± SE. *$P < 0.05$; **$P < 0.001$.

those of diabetic ICAM-1–deficient mice, which lacked prominent macrophage infiltration into kidney tissue (10). Cell adhesion assay confirmed that SR-A mediates adhesion of monocytes to type IV collagen but not to endothelial cells. In addition, DNA microarray analysis revealed that proinflammatory genes were suppressed in the kidneys of DM-KO compared with DM-WT. The current results emphasize the role of macrophages in the pathogenesis of diabetic nephropathy and point to the contribution of SR-A to the progression of diabetic nephropathy through inflammatory process.

Macrophage infiltration into subendothelial space occurs through several steps, including rolling, sticking, and transmigration. ICAM-1 is known to contribute to macrophage sticking on endothelial cells. In our study, we confirmed equally overexpressed ICAM-1 in both DM-WT and DM-KO (data not shown). Furthermore, anti–SR-A mAb did not block macrophage adhesion on endothelial cells. Taken together, SR-A does not seem to modulate ICAM-1 expression or ICAM-1–mediated macrophage adhesion. Fraser et al. (32) first proposed a novel function of SR-A as a cell adhesion molecule. They provided a mechanism for mononuclear phagocyte recruitment to ligand-rich tissues such as in atherosclerotic lesions by SR-A. They observed that rat mAb against murine SR-A I and II (2F8) totally abolished divalent cation-independent adhesion of murine macrophages to tissue culture plastic. In addition, peritoneal macrophage from SR-A$^{-/-}$ mice displayed reduced adhesion and spread over the first 24 h after isolation (15). SR-A is known to bind to the following extracellular matrix components: glycated collagen IV (33), denatured type I collagen, native type IV collagen (34), and fucoidan (13). Considered together, SR-A seems to play a central role in trapping monocytes in the subendothelial space in various conditions such as atherosclerosis and diabetic nephropathy.

It was striking that UACR and glomerular hypertrophy of DM-WT progressed increasingly, whereas DM-KO presented gradual changes. These phenomena might reflect the intensity of microinflammation caused by infiltrated macrophage, at least in part. However, UACR and glomerular size at 1 month was similar in both diabetic groups. We speculate that hemodynamic effect may be an important factor at an early phase of diabetic nephropathy in our model. We found a slight difference in type IV collagen levels between DM-WT and DM-KO. It might be exacerbated and accelerated in DM-WT by continuous inflammation in an extended observation period.

We performed DNA microarray analysis to compare gene expression profiles of the kidneys and found 48 genes that were upregulated in DM-WT but not in DM-KO. Interestingly, most of their functions were related to response to stimuli or defense and immune response, suggesting that proinflammatory genes are overexpressed in diabetic kidneys and suppressed by SR-A deficiency. Alteration of these gene expressions might be caused by functional changes of SR-A–deficient macrophage or reduced number of macrophages in the kidneys of DM-KO. Among these genes, renal expression of OPN showed a dramatic change between DM-KO and DM-WT. OPN is known to act as a chemokine and a proinflammatory cytokine. OPN is expressed in renal resident cells and regarded as one of the key molecules in the pathogenesis of diabetic nephropathy (30). Moreover, OPN is also expressed on activated macrophage or T-cell, coordinates macrophage migration and activation, and is required for cell-mediated inflammatory responses (35,36). It also stimulates expression of proinflammatory cytokines in macrophages (37,38). OPN seems to be involved in a vicious cycle of macrophage infiltration and inflammatory process in diabetic nephropathy, although further evaluation is needed to clarify the mechanism of reduction of OPN in SR-A$^{-/-}$ mice.

Recent studies have shown that SR-A binds to AGEs (19,20). Gal-3 is also known to be expressed on macrophage and acts as AGE receptor. Pugliese et al. (39) reported that Gal-3 knockout mice developed accelerated glomerulopathy compared with wild-type animals. They speculated that overexpressed RAGE exacerbated progression of diabetic nephropathy in their model. In our study, RAGE expression was increased in diabetic kidney without significant difference between DM-WT and DM-KO.

Another possible mechanism is reduced oxidative stress. Several studies indicated that SR-A increased H_2O_2 secretion through interaction with CD36 (40,41). We noticed that SR-A$^{-/-}$ mice exhibit reduced oxidative stress, as suggested by lipid peroxide concentration. The reduction rate of lipid peroxides in DM-KO was as much as 42% of DM-WT. This finding might be due to lack of SR-A and its interaction with CD36 to generate reactive oxygen species.

Body weight of DM-KO was slightly higher than DM-WT, although metabolic data, including A1C and blood glucose, were not different between the two groups. Interestingly, these results are also consistent with those in ICAM-1–deficient mice, although the mechanism remains unclear (10). Babaev et al. (16) also reported that irradiated C57/BL6 mice reconstituted with SR-A$^{-/-}$ macrophages revealed body weight gain.

The control of the inflammatory process might be a potential strategy for attenuating the progression of diabetic nephropathy. Utimura et al. (42) reported that long-term anti-inflammatory therapy ameliorated experimental diabetic nephropathy in rats. Recent studies from our laboratories also revealed that the anti-inflammatory agents could ameliorate experimental diabetic nephropathy through inhibition of the inflammatory process, such as expression of ICAM-1 and macrophage infiltration (43–45).

In conclusion, our results suggest that SR-A promotes macrophage migration into diabetic kidneys by mediating the attachment to renal extracellular matrix, including basement membranes and mesangial matrix. SR-A may be a key molecule for the inflammatory process in pathogenesis of diabetic nephropathy and a novel therapeutic target for diabetic vascular complications.

ACKNOWLEDGMENTS

We are grateful for Dr. Hiroshi Suzuki (National Research Center for Protozoan Diseases, Obihiro University of Agriculture and Veterinary Medicine, Obihiro, Japan) and Chugai Research Institute for Medical Science, INC Pharmacology & Pathology Research Center (Shizuoka, Japan) for the supply of SR-A knockout mice. We appreciate Dr. Akito Izumi and Dr. Kenji Inoue (Laboratory for System Biology and Medicine, The Research Center for Advanced Science and Technology, the University of Tokyo, Japan) for performing microarray assay. We appreciate Dr. Itaru Kataoka for technical support.

A part of this study was presented at International Maillard Symposium (2001), and its proceeding was presented in Annals of the New York Academy and Sciences (2005).

REFERENCES

1. Koya D, Jirousek MR, Lin YW, Ishii H, Kuboki K, King GL: Characterization of protein kinase C beta isoform activation on the gene expression of transforming growth factor-beta, extracellular matrix components, and prostanoids in the glomeruli of diabetic rats. *J Clin Invest* 100:115–126, 1997
2. Ziyadeh FN, Sharma K, Ericksen M, Wolf G: Stimulation of collagen gene expression and protein synthesis in murine mesangial cells by high glucose is mediated by autocrine activation of transforming growth factor-beta. *J Clin Invest* 93:536–542, 1994
3. Vlassara H, Striker LJ, Teichberg S, Fuh H, Li YM, Steffes M: Advanced glycation end products induce glomerular sclerosis and albuminuria in normal rats. *Proc Natl Acad Sci U S A* 91:11704–11708, 1994
4. Brownlee M, Cerami A, Vlassara H: Advanced glycosylation end products in tissue and the biochemical basis of diabetic complications. *N Engl J Med* 318:1315–1321, 1988
5. Saraheimo M, Teppo AM, Forsblom C, Fagerudd J, Groop PH: Diabetic nephropathy is associated with low-grade inflammation in type 1 diabetic patients. *Diabetologia* 46:1402–1407, 2003
6. Nelson CL, Karschimkus CS, Dragicevic G, Packham DK, Wilson AM, O'Neal D, Becker GJ, Best JD, Jenkins AJ: Systemic and vascular inflammation is elevated in early IgA and type 1 diabetic nephropathies and relates to vascular disease risk factors and renal function. *Nephrol Dial Transplant* 20:2420–2426, 2005
7. Furuta T, Saito T, Ootaka T, Soma J, Obara K, Abe K, Yoshinaga K: The role of macrophages in diabetic glomerulosclerosis. *Am J Kidney Dis* 21:480–485, 1993
8. Hirata K, Shikata K, Matsuda M, Akiyama K, Sugimoto H, Kushiro M, Makino H: Increased expression of selectins in kidneys of patients with diabetic nephropathy. *Diabetologia* 41:185–192, 1998
9. Sugimoto H, Shikata K, Hirata K, Akiyama K, Matsuda M, Kushiro M, Shikata Y, Miyatake N, Miyasaka M, Makino H: Increased expression of intercellular adhesion molecule-1 (ICAM-1) in diabetic rat glomeruli: glomerular hyperfiltration is a potential mechanism of ICAM-1 upregulation. *Diabetes* 46:2075–2081, 1997
10. Okada S, Shikata K, Matsuda M, Ogawa D, Usui H, Kido Y, Nagase R, Wada J, Shikata Y, Makino H: Intercellular adhesion molecule-1-deficient mice are resistant against renal injury after induction of diabetes. *Diabetes* 52:2586–2593, 2003
11. Kodama T, Freeman M, Rohrer L, Zabrecky J, Matsudaira P, Krieger M: Type I macrophage scavenger receptor contains alpha-helical and collagen-like coiled coils. *Nature* 343:531–535, 1990
12. Platt N, Gordon S: Is the class A macrophage scavenger receptor (SR-A) multifunctional? The mouse's tale. *J Clin Invest* 108:649–654, 2001
13. Santiago-Garcia J, Kodama T, Pitas RE: The class A scavenger receptor binds to proteoglycans and mediates adhesion of macrophages to the extracellular matrix. *J Biol Chem* 278:6942–6946, 2003
14. Coller SP, Paulnock DM: Signaling pathways initiated in macrophages after engagement of type A scavenger receptors. *J Leukoc Biol* 70:142–148, 2001
15. Suzuki H, Kurihara Y, Takeya M, Kamada N, Kataoka M, Jishage K, Ueda O, Sakaguchi H, Higashi T, Suzuki T, Takashima Y, Kawabe Y, Cynshi O, Wada Y, Honda M, Kurihara H, Aburatani H, Doi T, Matsumoto A, Azuma S, Noda T, Toyoda Y, Itakura H, Yazaki Y, Kodama T, et al.: A role for macrophage scavenger receptors in atherosclerosis and susceptibility to infection. *Nature* 386:292–296, 1997
16. Babaev VR, Gleaves LA, Carter KJ, Suzuki H, Kodama T, Fazio S, Linton MF: Reduced atherosclerotic lesions in mice deficient for total or macrophage-specific expression of scavenger receptor-A. *Arterioscler Thromb Vasc Biol* 20:2593–2599, 2000
17. de Winther MP, van Dijk KW, Havekes LM, Hofker MH: Macrophage scavenger receptor class A: a multifunctional receptor in atherosclerosis. *Arterioscler Thromb Vasc Biol* 20:290–297, 2000
18. Araki N, Higashi T, Mori T, Shibayama R, Kawabe Y, Kodama T, Takahashi K, Shichiri M, Horiuchi S: Macrophage scavenger receptor mediates the endocytic uptake and degradation of advanced glycation end products of the Maillard reaction. *Eur J Biochem* 230:408–415, 1995
19. Uesugi N, Sakata N, Horiuchi S, Nagai R, Takeya M, Meng J, Saito T, Takebayashi S: Glycoxidation-modified macrophages and lipid peroxidation products are associated with the progression of human diabetic nephropathy. *Am J Kidney Dis* 38:1016–1025, 2001
20. Fukuhara-Takaki K, Sakai M, Sakamoto Y, Takeya M, Horiuchi S: Expression of class A scavenger receptor is enhanced by high glucose in vitro and under diabetic conditions in vivo: one mechanism for an increased rate of atherosclerosis in diabetes. *J Biol Chem* 280:3355–3364, 2005
21. Eisen MB, Spellman PT, Brown PO, Botstein D: Cluster analysis and display of genome-wide expression patterns. *Proc Natl Acad Sci U S A* 95:14863–14868, 1998
22. Ashburner M, Ball CA, Blake JA, Botstein D, Butler H, Cherry JM, Davis AP, Dolinski K, Dwight SS, Eppig JT, Harris MA, Hill DP, Issel-Tarver L, Kasarskis A, Lewis S, Matese JC, Richardson JE, Ringwald M, Rubin GM, Sherlock G, The Gene Ontology Consortium: Gene ontology: tool for the unification of biology. *Nat Genet* 25:25–29, 2000
23. Dennis G Jr, Sherman BT, Hosack DA, Yang J, Gao W, Lane HC, Lempicki RA: DAVID: Database for annotation, visualization, and integrated discovery. *Genome Biol* 4:P3, 2003
24. Tomokiyo R, Jinnouchi K, Honda M, Wada Y, Hanada N, Hiraoka T, Suzuki H, Kodama T, Takahashi K, Takeya M: Production, characterization, and interspecies reactivities of monoclonal antibodies against human class A macrophage scavenger receptors. *Atherosclerosis* 161:123–132, 2002
25. Kataoka N, Iwaki K, Hashimoto K, Mochizuki S, Ogasawara Y, Sato M, Tsujioka K, Kajiya F: Measurements of endothelial cell-to-cell and cell-to-substrate gaps and micromechanical properties of endothelial cells during monocyte adhesion. *Proc Natl Acad Sci U S A* 99:15638–15643, 2002
26. Shikata Y, Birukov KG, Birukova AA, Verin A, Garcia JG: Involvement of site-specific FAK phosphorylation in sphingosine-1 phosphate- and thrombin-induced focal adhesion remodeling: role of Src and GIT. *FASEB J* 17:2240–2249, 2003
27. Cancello R, Henegar C, Viguerie N, Taleb S, Poitou C, Rouault C, Coupaye M, Pelloux V, Hugol D, Bouillot JL, Bouloumie A, Barbatelli G, Cinti S, Svensson PA, Barsh GS, Zucker JD, Basdevant A, Langin D, Clement K: Reduction of macrophage infiltration and chemoattractant gene expression changes in white adipose tissue of morbidly obese subjects after surgery-induced weight loss. *Diabetes* 54:2277–2286, 2005
28. Hsieh TJ, Chen R, Zhang SL, Liu F, Brezniceanu ML, Whiteside CI, Fantus IG, Ingelfinger JR, Hamet P, Chan JS: Upregulation of osteopontin gene expression in diabetic rat proximal tubular cells revealed by microarray profiling. *Kidney Int* 69:1005–1015, 2006
29. Kelly DJ, Wilkinson-Berka JL, Ricardo SD, Cox AJ, Gilbert RE: Progression of tubulointerstitial injury by osteopontin-induced macrophage recruitment in advanced diabetic nephropathy of transgenic (mRen-2) 27 rats. *Nephrol Dial Transplant* 17:985–991, 2002
30. Susztak K, Bottinger E, Novetsky A, Liang D, Zhu Y, Ciccone E, Wu D, Dunn S, McCue P, Sharma K: Molecular profiling of diabetic mouse kidney

reveals novel genes linked to glomerular disease. *Diabetes* 53:784–794, 2004
31. Kelly DJ, Chanty A, Gow RM, Zhang Y, Gilbert RE: Protein kinase C beta inhibition attenuates osteopontin expression, macrophage recruitment, and tubulointerstitial injury in advanced experimental diabetic nephropathy. *J Am Soc Nephrol* 16:1654–1660, 2005
32. Fraser I, Hughes D, Gordon S: Divalent cation-independent macrophage adhesion inhibited by monoclonal antibody to murine scavenger receptor. *Nature* 364:343–346, 1993
33. el Khoury J, Thomas CA, Loike JD, Hickman SE, Cao L, Silverstein SC: Macrophages adhere to glucose-modified basement membrane collagen IV via their scavenger receptors. *J Biol Chem* 269:10197–10200, 1994
34. Gowen BB, Borg TK, Ghaffar A, Mayer EP: The collagenous domain of class A scavenger receptors is involved in macrophage adhesion to collagens. *J Leukoc Biol* 69:575–582, 2001
35. Weber GF, Zawaideh S, Hikita S, Kumar VA, Cantor H, Ashkar S: Phosphorylation-dependent interaction of osteopontin with its receptors regulates macrophage migration and activation. *J Leukoc Biol* 72:752–761, 2002
36. Khajoee V, Saito M, Takada H, Nomura A, Kusuhara K, Yoshida S-I, Yoshikai Y, Hara T: Novel roles of osteopontin and CXC chemokine ligand 7 in the defence against mycobacterial infection. *Clin Exp Immunol* 143:260–268, 2006
37. Suzuki K, Zhu B, Rittling SR, Denhardt DT, Goldberg HA, McCulloch CA, Sodek J: Colocalization of intracellular osteopontin with CD44 is associated with migration, cell fusion, and resorption in osteoclasts. *J Bone Miner Res* 17:1486–1497, 2002
38. Zhu B, Suzuki K, Goldberg HA, Rittling SR, Denhardt DT, McCulloch CA, Sodek J: Osteopontin modulates CD44-dependent chemotaxis of peritoneal macrophages through G-protein-coupled receptors: evidence of a role for an intracellular form of osteopontin. *J Cell Physiol* 198:155–167, 2004
39. Pugliese G, Pricci F, Iacobini C, Leto G, Amadio L, Barsotti P, Frigeri L, Hsu DK, Vlassara H, Liu FT, Di Mario U: Accelerated diabetic glomerulopathy in galectin-3/AGE receptor 3 knockout mice. *FASEB J* 15:2471–2479, 2001
40. Maxeiner H, Husemann J, Thomas CA, Loike JD, El Khoury J, Silverstein SC: Complementary roles for scavenger receptor A and CD36 of human monocyte-derived macrophages in adhesion to surfaces coated with oxidized low-density lipoproteins and in secretion of H2O2. *J Exp Med* 188:2257–2265, 1998
41. Jozefowski S, Kobzik L: Scavenger receptor A mediates H2O2 production and suppression of IL-12 release in murine macrophages. *J Leukoc Biol* 76:1066–1074, 2004
42. Utimura R, Fujihara CK, Mattar AL, Malheiros DM, Noronha IL, Zatz R: Mycophenolate mofetil prevents the development of glomerular injury in experimental diabetes. *Kidney Int* 63:209–216, 2003
43. Usui H, Shikata K, Matsuda M, Okada S, Ogawa D, Yamashita T, Hida K, Satoh M, Wada J, Makino H: HMG-CoA reductase inhibitor ameliorates diabetic nephropathy by its pleiotropic effects in rats. *Nephrol Dial Transplant* 18:265–272, 2003
44. Yozai K, Shikata K, Sasaki M, Tone A, Ohga S, Usui H, Okada S, Wada J, Nagase R, Ogawa D, Shikata Y, Makino H: Methotrexate prevents renal injury in experimental diabetic rats via anti-inflammatory actions. *J Am Soc Nephrol* 16:3326–3338, 2005
45. Tone A, Shikata K, Sasaki M, Ohga S, Yozai K, Nishishita S, Usui H, Nagase R, Ogawa D, Okada S, Shikata Y, Wada J, Makino H: Erythromycin ameliorates renal injury via anti-inflammatory effects in experimental diabetic rats. *Diabetologia* 48:2402–2411, 2005